Active Modular Elastomer Sleeve for Soft Wearable Assistance Robots

Yong-Lae Park, Bor-rong Chen, Carmel Majidi, Robert J. Wood, Radhika Nagpal, and Eugene Goldfield

Abstract— A proposed adaptive soft orthotic device performs motion sensing and production of assistive forces with a modular, pneumatically-driven, hyper-elastic composite. Wrapping the material around a joint will allow simultaneous motion sensing and active force response through shape and rigidity control. This monolithic elastomer sheet contains a series of miniaturized pneumatically-powered McKibben-type actuators that exert tension and enable adaptive rigidity control. The elastomer is embedded with conductive liquid channels that detect strain and bending deformations induced by the pneumatic actuators. In addition, the proposed system is modular and can be configured for a diverse range of motor tasks, joints, and human subjects. This modular functionality is accomplished with a decentralized network of self-configuring nodes that manage the collection of sensory data and the delivery of actuator feedback commands. This paper mainly describes the design of the soft orthotic device as well as actuator and sensor components. The characterization of the individual sensors, actuators, and the integrated device is also presented.

Fig. 1. Overall structure of the modular active elastomer sleeve prototype.

I. INTRODUCTION

An estimate of 11.4% of Americans 15 years or older struggle with walking or climbing stairs and about 8% have limited upper body mobility [1]. These physical disabilities may be congenital or acquired and arise from a broad range of neuromuscular and skeletal impairments. Common sources include stroke, traumatic brain injury, spinal injury, amputation, muscular dystrophy (MD), and cerebral palsy (CP). In many cases, motor impairment can dramatically impact health, livelihood, and quality of life and lead to secondary medical disorders and physical dependency [2].

Assistive technologies such as electrically powered prosthetics [3], [4], [5], orthotic exoskeletons [6], [7], [8], [9], and medical robotics can dramatically improve motor independence and rehabilitation. Such technologies have the poten-

Y.-L. Park is with the Wyss Institute for Biologically Inspired Engineering, Harvard University, Boston, MA 02115 USA (e-mail: yl-park@wyss.harvard.edu).

B. Chen is with the School of Engineering and Applied Science, Harvard University, Cambridge, MA 02138 USA (e-mail: brchen@eecs.harvard.edu).

C. Majidi is with the Department of Mechanical Engineering, Carnegie Mellon University, Pittsburgh, PA 15213 USA (e-mail: cmajidi@andrew.cmu.edu).

R. J. Wood and R. Nagpal are with the School of Engineering and Applied Science, Harvard University, Cambridge, MA 02138 USA, and also with the Wyss Institute for Biologically Inspired Engineering, Harvard University, Boston, MA 02115 USA (rjwood@eecs.harvard.edu; rad@eecs.harvard.edu).

E. C. Goldfield is with the Children's Hospital Boston, Boston, MA 02115, and also with the the Wyss Institute for Biologically Inspired Engineering, Harvard University, Boston, MA 02115 USA (e-mail: Eugene.Goldfield@childrens.harvard.edu).
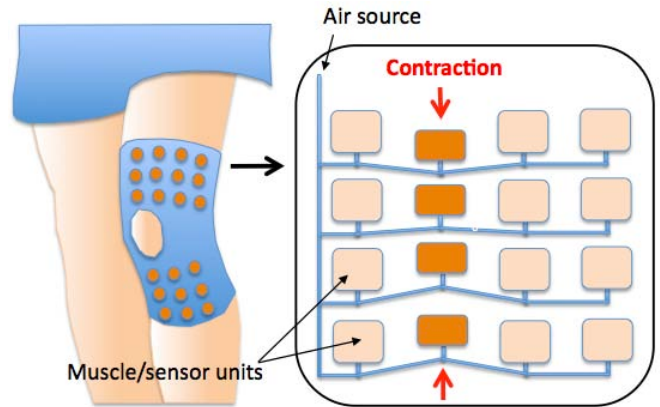
tial to restore or compensate for lost function and, in the case of congenital impairments like MD or CP, promote normal motor development. Progress, however, will depend on new assistive technologies that are comfortable to wear, safe, and compatible with human motion and mechanics. For most applications, this requires a transition from conventional electronics and motors, which are rigid and inextensible, to active materials that are elastically stretchable and match the soft compliance of human skin and tissue.

We address this fundamental demand by introducing a programmable orthotic device that is intrinsically soft, wearable, pneumatically powered, and modular. When worn around a joint such as a wrist or knee, the orthotic will electronically monitor body motion and assist with motor function. In contrast to existing active orthotics [6], [8], [9], [10] and exoskeletons [7], [11], this device is soft, modular, multifunctional, and composed almost entirely of elastomer and embedded micro-fluidic channels. This builds on work in soft robotics [8], [12], [13], [14], [15] and embedded sensing [16], [17], [18], [19]. These unique properties will allow the soft orthotic to support a broad range of motor tasks and function reliably under extreme loads and body movements.

As illustrated in Fig. 1, the soft robot contains an array of independently controlled nodes. Each node contains an actuator that controls rigidity and contraction, a sensor that monitors the output of the actuator, and digital circuitry for control and communication. When wrapped around a joint, this mesh of actuators and sensors can monitor and assist in both lower and upper body tasks.

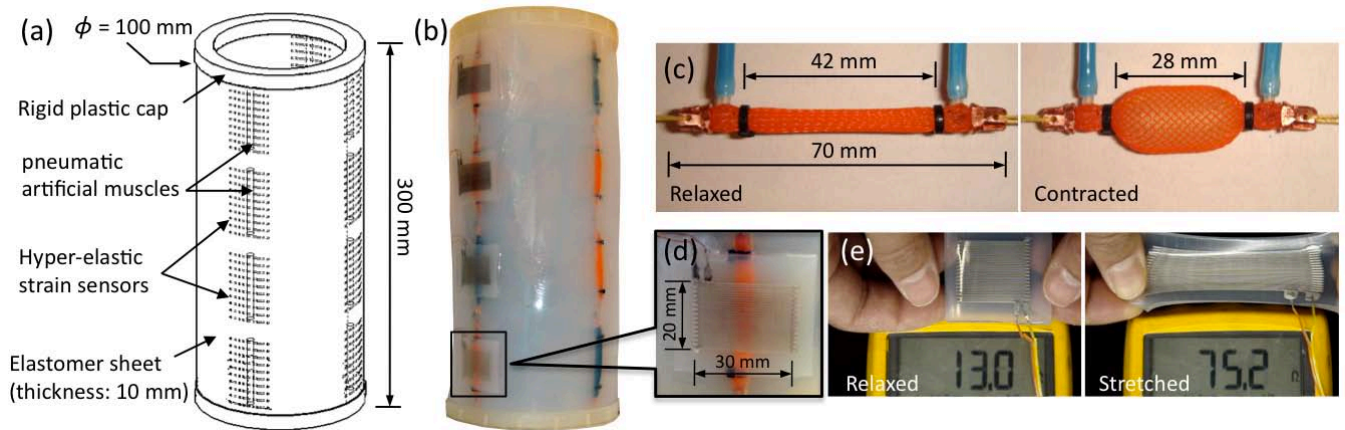In this manuscript, we begin with an overview of the prototype design and fabrication including the node design,

Fig. 2. (a) Prototype design. (b) Actual prototype (c) Custom-built miniaturized McKibben pneumatic artificial muscle. (d) Magnified view of strain sensor integrated pneumatic muscle. (e) Custom-built hyper-elastic strain sensor.

mesh topology, and software architecture (Section II). In Section IV, we present the mathematical theories and design principles for the actuation and sensing elements of the soft orthotic. This is followed in Section V with the characterization of the prototype comprised of sixteen independently controlled actuators. We close with a discussion (Section VI) and concluding remarks (Section VII) that review the current results, challenges, and outlook for programmable soft orthotics.

II. DESIGN

A. Mechanical Design

The overall structure of the device is a three-dimensional soft cylindrical sleeve (Fig. 1) with embedded soft pneumatic artificial muscles and strain sensors. When multiple muscles are actuated (contracted) collectively as a group, the overall displacement and force produced will be relatively high. The extremely flexible and elastic base material, a silicone elastomer, makes the prototype conformable to the tapered cylindrical forms of human body segments. Each pneumatic muscle is equipped with a soft strain sensor that detects the contraction of the pneumatic muscle. Four muscle cells with strain sensors are controlled by one micro-controller as one modular unit.

Fig. 2 shows the design and actual prototype of the device. The base material is silicon elastomer[1], and the actuators and sensors are embedded in the elastomer. The current prototype has four modular units with 16 muscles (4 rows × 4 columns) in total. Each actuator is connected to two off-the-shelf miniature solenoids valves[2] for compressed air injection and release, respectively. Although the ultimate goal is that each actuator has its own strain sensor, we decided to have strain sensors integrated only in one actuator column (four actuators) in the current prototype. The weight of the current prototype is approximately 1.2 kg. With different combinations of artificial muscle contractions, various shapes can be achieved, as shown in Fig. 3 and Fig. 4
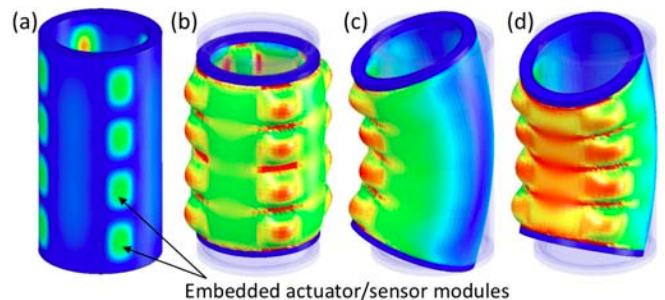

Fig. 3. Examples of shape changes of the active elastomer sleeve by simulation. (a) Original shape. (b) Whole body contraction. (c) and (d) Partial contractions for bending.

1) Actuation: Miniaturized McKibben-type pneumatic synthetic muscles were built and used as main actuators (Fig. 2(c)). A latex tube with air fittings was enclosed in an expandable mesh sleeve[3], and the ends of of the mesh were clamped. When pressurized air is introduced to the latex tube through the air fitting, the mesh sleeve allows expansion in radial directions while creating contraction in its axial direction.

2) Sensing: Four pneumatic muscles are equipped with a hyper-elastic strain sensor (Fig. 2(d)) to measure the actuator contraction. The strain sensor consists of a micro-channel filled with liquid metal (EGaIn) that changes overall resistance of the channel as the sensor experiences strain changes [8], [14], [15]. Since each strain sensor is placed perpendicular to the axial direction of the corresponding pneumatic muscle, the strain sensor detects the radial expansion of the actuator, as shown in Fig. 2(a), and, the strain information needs to be converted to the contraction length of the muscle.

B. Programmable Controller Network

1) Controller Network Topology: A network of programmable micro-controllers[4] controls the soft orthotic mod-
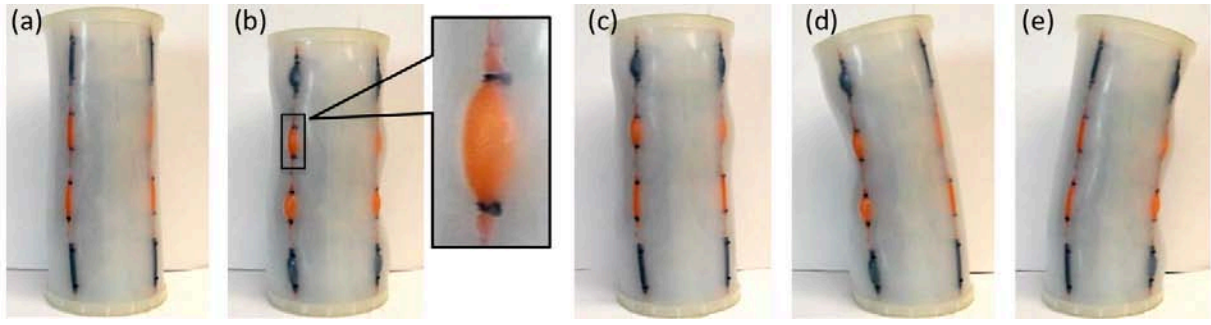
Fig. 4. Prototype in action showing different shape changes. (a) Original shape without actuation. (b) Whole body contraction with a magnified view of a contracted artificial muscle. (c) Partial contraction (only the 1st and 2nd rows from the top are actuated.). (d), (e) Partial contractions for bending (only two adjacent columns are actuated.).

ular units in the soft orthotic. The controllers are connected in a two-dimensional mesh pattern, both spatially and logically, as illustrated in Fig. 1. Global motion patterns of the device are carried out by scheduled tasks that run on the network of controllers. In this topology, each controller has four neighboring controllers that it can directly communicate with, using four dedicated serial communication ports. Therefore, the network of controllers provides the computation platform that hosts higher level intelligent processing, interpretation, and timely detection of global patterns from real-time signals within the orthotic.

2) System Software Architecture: Fig. 5(a) shows the controller software architecture. The architecture is divided into two main layers: System Services Layer, and Application Layer. The System Services Layer implements fundamental components that manage local resources and provide primitives to support algorithms at the Application Layer. The System Services Layer implements a clock-driven scheduler, handles inter-module communication with neighboring modules, processes readings from strain sensors, and sets actuation parameters. The Application Layer specifies the application goal using the services provided by the System Services Layer.

3) Clock-driven scheduling: We adopt a clock-driven scheduling approach to schedule software tasks at fixed time slots to provide predictable execution of specific tasks at individual modular units. As Fig. 5(b) shows, all computational tasks are scheduled to run at fixed schedules. Such structure allows simplification of control on timing of sensing, processing, and actuation tasks. At the Application Layer, the timing of tasks is configurable to fit application specific goals.

4) Global Control Program Structure: Leveraging the services outlined above, the orthotic device can be programmed to perform desired motion patterns. The motions are described as scheduled tasks on multiple microcontrollers.

III. FABRICATION

After preparing all the components, such as sensors and actuators, they are integrated into a device that is shown in Fig. 2(b). The fabrication process can be divided into three steps.
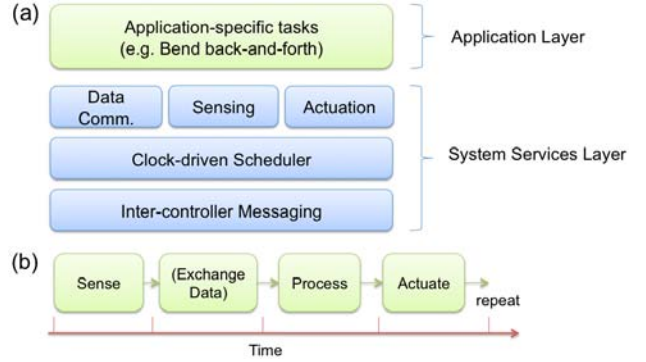

Fig. 5. (a) Software architecture. (b) Controller programs are specified as statically scheduled tasks.

The first step is to cast a flat elastomer sheet with embedded actuators and sensors. In this step, four actuators are tied in series through kevlar fibers, and four actuator groups are placed in parallel in a flat mold. Then, liquid polymer is poured. The strain sensors are connected through thin and flexible copper wires that ensures the electrical connection during different motions of the device.

The second step is to make the cured elastomer sheet a cylindrical shape. The flat elastomer sheet is curled and placed in a semicylindrical mold, and small amount of liquid polymer is poured inside of the curled elastomer cylinder to make a seam.

The final step is to assemble the plastic caps to the both ends of the cylinder. The kevlar fibers from the end of each actuator column are fixed to the cap to ensure the desired motions of the cylinder with contraction.

Since each actuator is equipped with its own solenoid valves, it can be individually controlled for contraction and release.

IV. THEORY

In order to monitor and assist human joint motion, the soft orthotic must be designed to register strains and produce forces that are comparable to those of natural muscle. Design is based on principles of mechanics, which govern the strain response, power output, and rigidity of the modular elements.

We tune these properties by selecting the appropriate materials, geometries, and operating pressures.

A. Pneumatic Artificial Muscle Actuator

Each node of the modular array contains a McKibben-type pneumatic actuator that controls both the natural length and rigidity of the node. The actuator is composed of an inextensible thread of length b wrapped around a rubber cylinder that has a natural length L_0, radius R_0, and elastic modulus E. The thread has a pitch $\theta_0 = cos^{-1}(L_0/b)$ and is wrapped $n = bsin(\theta_0)/2\pi R_0$ times around the cylinder [20]. Since b and n are both fixed, the kinematics of the actuator are restricted to a single free parameter: the length L of the actuator at static equilibrium.

Under a tensile load F, the total potential energy of the actuator has the form

$$U = U(L) = -P\pi R^2 L - FL + \frac{\pi EhRL}{1-v}\{\varepsilon_\psi^2 + \varepsilon_n^2 + 2v\varepsilon_\psi\varepsilon_n\} \quad (1)$$

where

$$R = \sqrt{\frac{b^2 - L^2}{2\pi n}}, \varepsilon_\psi = \frac{R^2 - R_0^2}{2R_0^2}, \varepsilon_n = \frac{L^2 - L_0^2}{2L_0^2}, \quad (2)$$

h is the thickness of the cylindrical wall, and $v = 1/2$ is its Poissons ratio. At equilibrium, U must be stationary with respect to L such that $dU/dL = 0$. However, determining L at equilibrium requires solving a sixth order polynomial. Analysis is simplified by ignoring the elastic contribution of the rubber shell, i.e. $U = -P\pi R^2 L - FL$. In the absence of a tensile force F (i.e. F = 0), the equilibrium length of the actuator becomes $L^* = 0.577b$ for any value of $P > 0$.

Filling the actuator with a pressure $P > 0$ will cause the actuator to shorten from a length L_0 to a final length

$$L = \sqrt{\frac{1}{3}\left(\frac{2nF}{P} + b^2\right)}. \quad (3)$$

Suppose, for example, that the actuator is placed adjacent to a joint of radius λ. Inflating the actuator with a pressure P will cause the joint to rotate by an amount $\Delta\theta = (L_0 - L)/\lambda$. Here, F is replaced with M/λ, where M is the magnitude of applied torque. In the absence of an external torque, the joint will rotate by $(L_0 - 0.577b)/\lambda$ radians. From this new reference state, the torsional spring constant of the joint is $\kappa = 1.732Pb\lambda 2/n$.

For N actuators in parallel, the angle of rotation during contraction remains the same but the torsional spring constant (and torque required to prevent joint rotation) increases by a factor of N. In contrast, for N actuators in series, the angle or rotation increases by a factor of N but torsional rigidity reduces by a factor of N.

B. Strain Sensor

Joint motion and actuator contraction are monitored with strain sensors that are embedded in the host elastomer. The design of these sensors is based on the Whitney strain gauge and are composed of a rubber tube filled with conductive liquid [21]. As the tube stretches with a strain ε, the cross-section decreases and the electric resistance increases by a relative amount $2\varepsilon + \varepsilon^2$. For a strain sensor of length ζ placed around a joint of radius λ, a bending angle $\Delta\theta$ corresponds to a relative change in resistance of

$$\frac{\Delta R}{R} = \frac{2\lambda}{\zeta}\Delta\theta \quad (4)$$

If, for example, $\zeta = 0.1\lambda$, then a $10°$ bending angle results in a 3.4% increase in electric resistance.

C. Elastomer Design

In order to avoid interference with the body mechanics, the elastomer should exhibit approximately the same mechanical compliance as natural skin. The membrane stiffness of the elastomer is $S = EH$, where E is the elastic modulus and H is the elastomer thickness. Therefore, E and H must satisfy the condition $EH = E_sH_s$, where E_s and H_s are the modulus and thickness of natural skin, respectively. Hence, an elastomer with an elastic modulus on the order of skin (1 MPa) must share the same millimeter thickness as the epidermis.

Alternatively, elastomer stiffness may be represented in terms of the corresponding stiffness of a torsional spring. As the joint bends, the orthotic stretches and exerts a torque about the center of the joint. For a single module unit of thickness H, width w, and length ξ, the torsional spring constant will be $\kappa = EwH\lambda 2/\xi$, where λ is the joint radius. For a soft-as-skin orthotic, this torsional spring constant will be small compared to the natural joint stiffness. This assumption is reasonable since even natural skin has little influence on joint stiffness, which is instead governed by the elasticity of muscles, tendons, and subcutaneous tissue.

V. CHARACTERIZATION

The prototype was characterized in two different levels. The individual components, actuators and sensors, were first characterized, and then, the integrated device that has 16 embedded sensor-actuator units was characterized.

A. Actuator

The custom-built pneumatic artificial muscle was experimentally characterized. The McKibben pneumatic actuator shows different behaviors for different contraction rates and air pressures. A single actuator was fixed to a commercial materials tester[5], as shown in Fig. 6(a), and a constant air pressure was provided while maintaining the original muscle length. Then, the artificial muscle was gradually released at a rate of 2 mm/sec until the axial contraction force reached to 0. By repeating this experiment with varied air pressures, the contraction forces were measured with different contraction rates. The full characterization result is shown in Fig. 7.

When the air pressure was increased up to 550 kPa, the contraction rate increased up to 25% in the experiments. The maximum achievable force was approximately 93 N with a
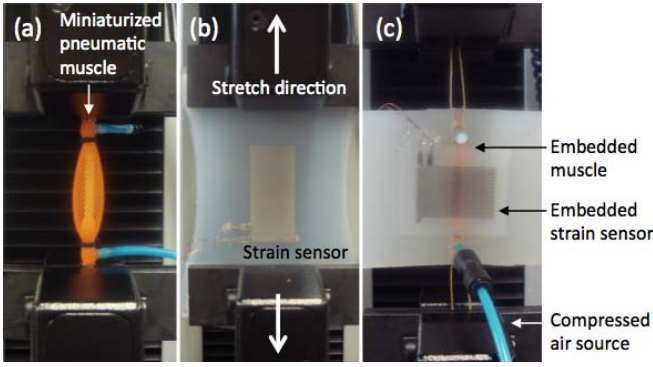
Fig. 6. Experimental setups for sensor and actuator characterization. (a) Single pneumatic muscle calibration setup. (b) Strain sensor calibration setup before being integrated with an actuator. (c) Single muscle-sensor integrated unit calibration setup.
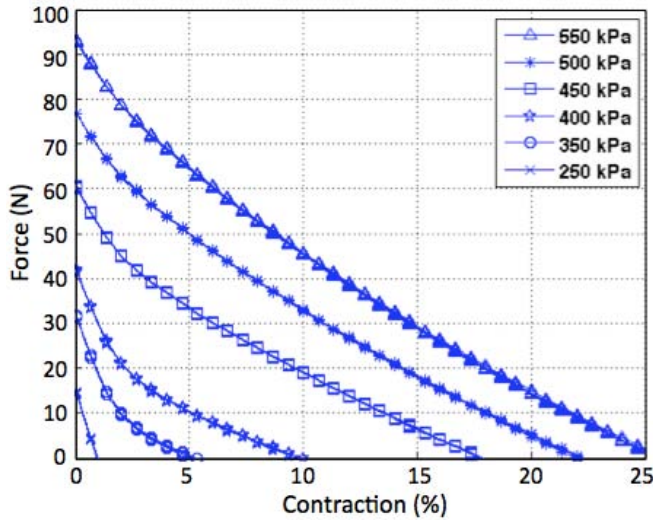

Fig. 7. Single actuator characterization plot.

Fig. 8. Strain sensor characterization results. (a) Strain response plot. (b) Sensor response plot for muscle actuation.

pressure of 550 kPa. More detailed characterization results can be found in [22].

Since the pneumatic muscle produces its maximum force at the start of contraction, it will be useful to initiate the joint motion when it cooperates with the user's biological muscles because biological muscles have minimum contraction force when they are fully stretched.

B. Sensor

The strain sensor was calibrated by applying axial strain up to 100% multiple times using a materials tester before being integrated with an actuator, as shown in Fig. 6(b). To check the hysteresis level of the sensor, the experiment included loading and unloading loops. The stretch and release rate was 0.5 mm/sec. Fig. 8(a) shows the calibration result. The nominal resistance at rest is 10.3 Ω. Assuming the thermal effect on the strain sensor is negligible, the experimental gauge factor is 3.37 based on the calibration result. The result shows a linear and repeatable strain response and negligible hysteresis.
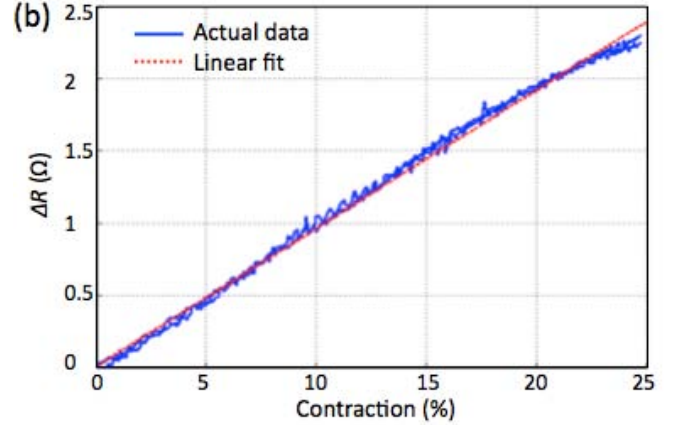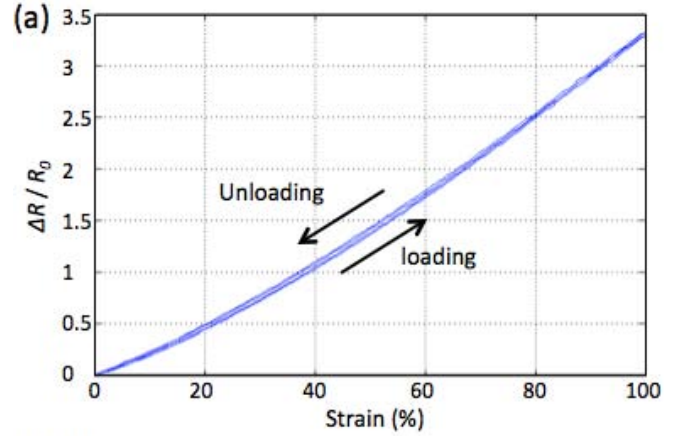
Once integrated with an actuator, as shown in Fig. 6(c), the strain sensor signal is used to measure the contraction of a single muscle. Fig. 8(b) shows the calibration result of a single sensor-actuator unit. The artificial muscle was contracted multiple times up to 25% of the original length from the relaxed state, and the resistance change of the strain sensor was measured. The result shows a linear response for measuring muscle contraction.

C. Device

The integrated device was characterized using four pneumatic muscles, in one column, which are equipped with strain sensors. The bending angle, ϕ, defined in Fig. 9(a), can be theoretically calculated from the diagram shown in Fig. 9(b). If the length of the four contraction sides are x_1, x_2, x_3, and x_4, respectively, assuming there are no length changes on the other sides (l) and the diameter of the cylinder (d), the location of the top center point, P, can be expressed relative to the bottom center point, $(0, 0)$ in the figure, of the cylinder as following:

$$P = (p_x, p_y) = \left(\sum_{i=1}^{4} y_i \cdot \sin \alpha_i , \sum_{i=1}^{4} y_i \cdot \cos \alpha_i \right) \quad (5)$$
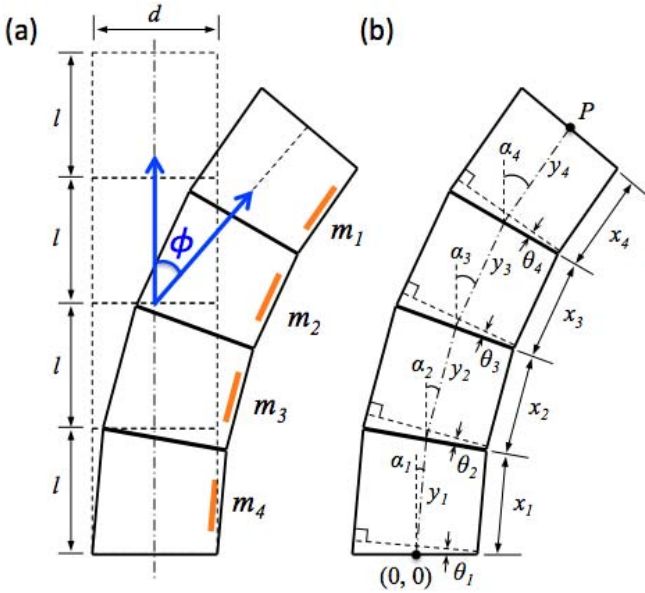
Fig. 9. (a) Definition of bending angle (ϕ) with contraction of four muscle-sensor units (m_1, m_2, m_3, and m_4). (b) Bending angle calculation of each row.

where

$$y_i = \frac{x_i + l}{2}, \ \alpha_1 = \theta_1, \text{ and } \alpha_n = 2\sum_{i=1}^{n-1} \theta_i + \theta_n \ (i \geq 2).$$

Then, the bending angle of the entire cylinder is:

$$\phi = \tan^{-1}\left(\frac{p_x}{p_y - 2l}\right). \tag{6}$$

Different bending angles were achieved in the following experiments. The angles are presented in three ways in the results (Figs. 10 to 13): desired angles that were theoretically calculated, estimated angles using the strain sensor information, and actual angles measured using a commercial video analysis software[6]. The source air pressure for actuation was 500 kPa with a flow rate of 0.5 cfm during the device characterization experiments.

1) Case 1: Contract four muscles simultaneously: All four muscles are simultaneously contracted to reach the desired target angle. Fig. 10 shows the result. The target angle is 15°, the estimated angle using the strain sensors is approximately 13°, and the actual achieved angle is approximately 11.5°.

2) Case 2: Contract four muscles in sequence: In this test, the four muscles are contracted in sequence. The strain sensor data in Fig. reffig-contractSeq(a) shows the sequence of the contraction. Since all four muscles are contracted eventually, the target angle is the same 15°. The estimated angle is approximately 13°, and the actual achieved angle is approximately 12°, as shown in Fig. 11(b). The data show that the muscles, as expected, contracted with 1 sec interval between consecutive actuations.

[6]ProAnalyst, Xcitex, Cambridge, MA 02141, USA.

3) Case 3: Contract muscles 1 and 3 only: Only Muscles 1 and 3 are contracted. Fig. 12 shows the result. The target angle is 6.5°, the estimated angle is approximately 4.5°, and the actual achieved angle is approximately 4°.

4) Case 4: Contract muscles 2 and 4 only: Muscles 2 and 4 are contracted instead of Muscles 1 and 3 in this test. Fig. 13 shows the result. The target angle is 10°, the estimated angle is approximately 9°, and the actual achieved angle is approximately 8°. Although the number of contracted muscles are the same as in Case 3, since muscles 2 and 4 are located in lower positions than muscles 1 and 3, the result shows higher achieved angle than in Case 3.

The maximum achievable bending angle was approximately 12° with contraction of four actuators in one column, and the peak torque the device can generate is approximately 6.5 Nm with a simultaneous contraction of two actuator columns. The actual achieved angles were always smaller than the estimated angles from the strain sensor signals, and the estimated angles were always smaller than the target angles calculated theoretically. There are two main reasons on these undershoot results. First, since each actuator is hand-made, all the actuators are not exactly in the same dimensions and performance. More controlled manufacturing method will minimize this effect. Second, the prototype does not maintain exactly the same diameter along the body length because of the hollow elastomer structure. Embedding a diagonal mesh of flexible but inextensible fibers will reduce this effect while still allowing structural softness and flexibility.

The oscillations shown in all the experimental data are from the waving effect of the device. The momentary contractions of the pneumatic actuators cause the entire device to shake, since the device has its own mass and is made of elastic material. However, once the device is wrapped around a human body, this oscillation effect will be significantly reduced.

VI. DISCUSSION

The proposed orthotic has two key characteristics: softness and modularity. Being soft makes the orthotic suitable for compliance matching with natural mechanics of a person's body. Its modularity further allows the orthotic to be reconfigurable, failure tolerant, and easily tailorable to different individuals.

Although the device is a hollow cylindrical structure made of a soft material, it still has several limitations to overcome to be fully wearable. First, the solenoid valves and relatively stiff air tubing materials reduce the wearability. Second, electric wires used in this prototype are not stretchable. Finally, the base material, silicone rubber, is not a breathable material. As an ongoing work, the authors are exploring new technologies that could enable soft valves and stretchable electronics design using conductive micro-fluidic channels. Investigation on more breathable materials is another future work.

The experiments in Section V show that, leveraging of modular nature of the device, the software can achieve the
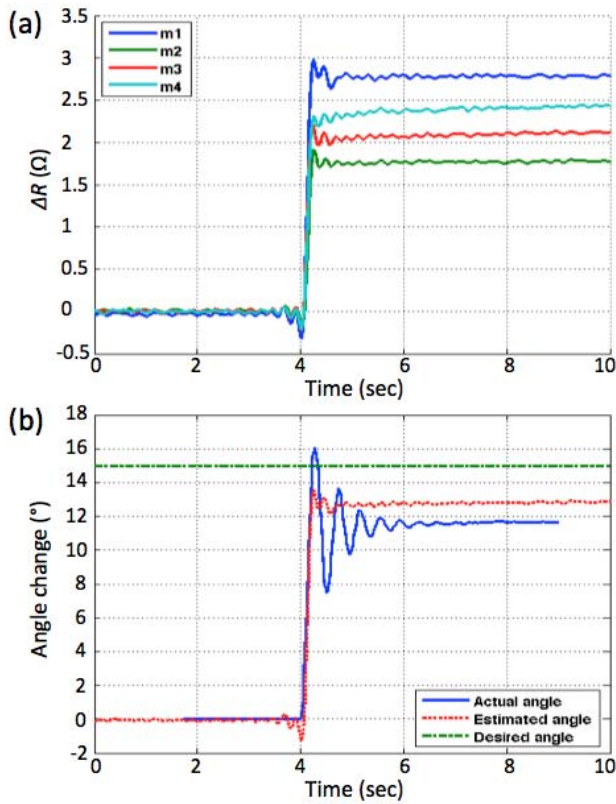
Fig. 10. Case 1: Contract all four muscles at once. (a) Strain sensor signals of the four actuation muscles. (b) Angle changes of the prototype.
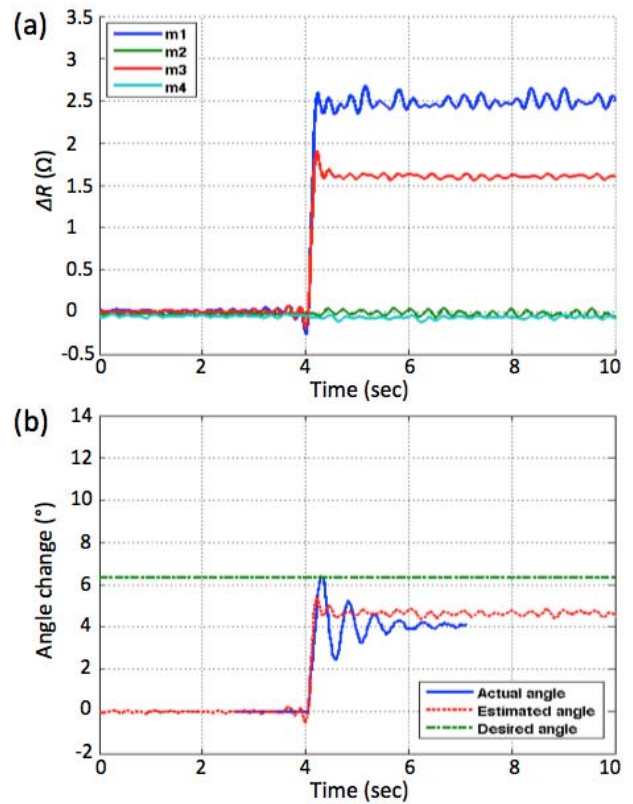

Fig. 12. Case 3: Contraction of muscles 1 and 3. (a) Strain sensor signals of the four actuation muscles. (b) Angle changes of the prototype.
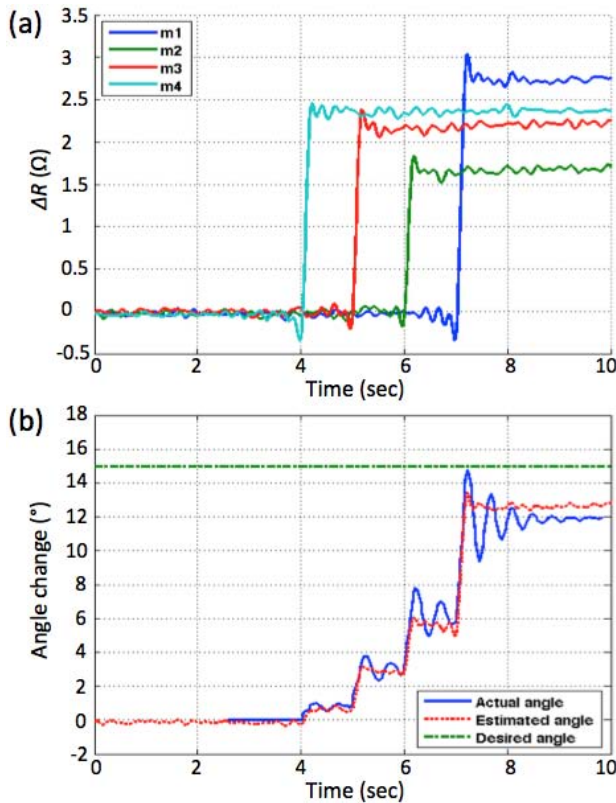

Fig. 11. Case 2: Contract four muscles in sequence. (a) Strain sensor signals of the four actuation muscles. (b) Angle changes of the prototype.
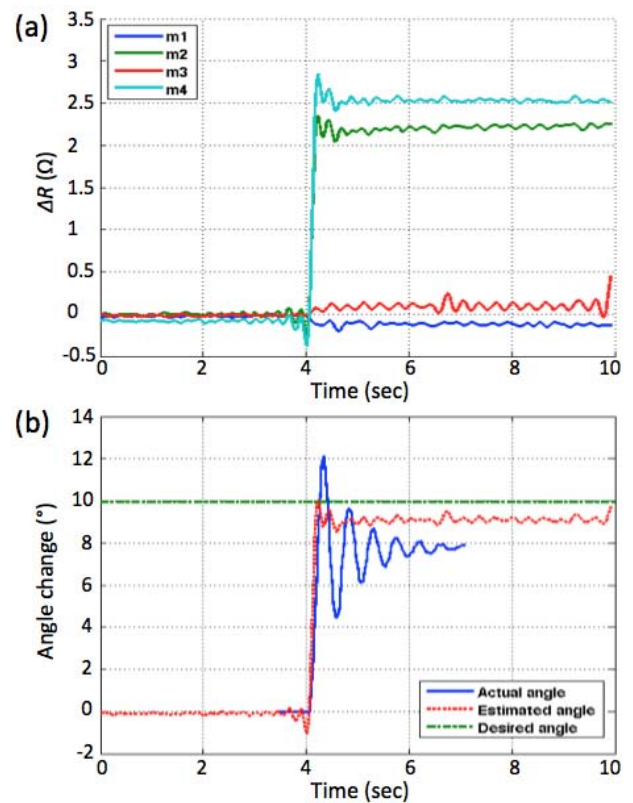

Fig. 13. Case 4: Contraction of muscles 2 and 4. (a) Strain sensor signals of the four actuation muscles. (b) Angle changes of the prototype.

similar actuation goals through multiple actuation plans. This is possible because the device is constructed from networked, independently controllable, and miniaturized muscles. This highlights an important feature: the orthotic can tolerate failures within the device. That is, when a particular actuation plan fails due to temporary or permanent damages of individual muscles within the device, the controller program can be designed such that it adapts to the failures by choosing an alternative actuation plan chosen to still achieve the target length or angle changes. To realistically benefit from this property, the controller programs must be designed to monitor if target actuation goals are reached, detect problematic units preventing successful actuation, and quickly switch to an alternative plan to compensate failures of a cell. Designing robust control strategies that take advantage of this property is part of our future work.

One important finding with our current prototype is that each individual muscle functions practically as a binary actuator due to the friction between the latex tube and the mesh sleeve. Significant axial contraction only happens when the pressure within the muscle overcomes the friction. In the future versions of this device, we will explore alternative designs, such as allowing proportional actuation of each individual muscle. Actuation at finer granularities will allow us to follow a bio-inspired design, in which the collective contributions of small, individual forces are added, or "recruited", until friction is overcome, and the actuation goal is achieved.

Although the current prototype relies on the lab-bench air source for pneumatic muscle actuation, the next version will be equipped with a small compressed air canister as an air source that makes the entire system fully portable.

VII. CONCLUSION

A modularized programmable active sleeve was developed using pneumatic actuators, hyper-elastic strain sensors, and an elastomer sheet. The prototype has 16 embedded pneumatic muscle cells and 4 hyper-elastic strain sensors. With different combinations of the actuations, the device is able to form various shapes in order to assist body motions. This is an initial step for building a wearable adaptive soft orthotic device. To achieve the final vision of adaptively and safely assisting human body movement, continuing research effort is necessary in developing adaptive control strategies, scalable manufacturing methods, and further miniaturization of muscle cells.

VIII. ACKNOWLEDGMENTS

REFERENCES

[1] E. Steinmetz, *Americans with disabilities: 2002*. Washington D.C.: U.S. Census Bureau, 2006.

[2] F. Miller, *Cerebral Palsy*, 1st ed. Springer, January 2005.

[3] S. K. Au, J. Weber, and H. Herr, "Powered ankle-foot prosthesis improves walking metabolic economy," *IEEE Trans. Rob.*, vol. 25, no. 1, pp. 51–66, February 2009.

[4] M. F. Eilenberg, H. Geyer, and H. Herr, "Control of a powered ankle-foot prosthesis based on a neuromuscular model," *IEEE Trans. Neural Syst. Rehabil. Eng.*, vol. 18, no. 2, pp. 164–173, Apr. 2010.

[5] B. G. Nascimento, C. B. S. Vimieiro, D. A. P. Nagem, and M. Pinotti, "Hip orthosis powered by pneumatic artificial muscle: Voluntary activation in absence of myoelectrical signal," *Artif. Organs*, vol. 32, no. 3, pp. 317–322, 2008.

[6] H. M. Herr and R. D. Kornbluh, "New horizons for orthotic and prosthetic technology: artificial muscle for ambulation," in *Proc. SPIE*, vol. 5385, 2004, pp. 1–9.

[7] D. P. Ferris, J. M. Czerniecki, and B. Hannaford, "An ankle-foot orthosis powered by artificial peumatic muscles," *J. Appl. Biomech.*, vol. 21, pp. 189–197, 2005.

[8] Y.-L. Park, B. Chen, D. Young, L. Stirling, R. J. Wood, E. Goldfield, and R. Nagpal, "Bio-inspired active soft orthotic device for ankle foot pathologies," in *Proc. IEEE/RSJ Int. Conf. Intell. Rob. Syst.*, San Francisco, CA, September 2011.

[9] L. Stirling, C. Yu, J. Miller, R. J. Wood, E. Goldfield, and R. Nagpal, "Applicability of shape memory alloy wire for an active, soft orthotic," *J. Mater. Eng. Perform.*, vol. 20, no. 4-5, pp. 658–662, 2011.

[10] H. Krebs, N. Hogan, W. Durfee, and H. Herr, "Rehabilitation robotics, orthotics, and prosthetics; chapter 48," *Textbook of Neural Repair and Rehabilitation (M. E. Selzer, S. Clarke, L. G. Cohen, P. W. Duncan, and F. H. Gage), Cambridge University Press*, 2005.

[11] K. E. Gordon, G. S. Sawicki, and D. P. Ferris, "Mechanical performance of artificial pneumatic muscles to power an ankle-foot orthosis," *J. Biomech.*, vol. 39, pp. 1832–1841, 2006.

[12] C. Majidi, R. Kramer, and R. J. Wood, "A non-differential elastomer curvature sensor for softer-than-skin electronics," *Smart Mater. Struct.*, vol. 20, no. 10, p. 105017, 2011.

[13] K. Noda, E. Iwase, K. Matsumoto, and I. Shimoyama, "Stretchable liquid tactile sensor for robot joints," in *Proc. IEEE Int. Conf. Rob. Autom.*, Anchorage, AK, May 2010.

[14] Y.-L. Park, C. Majidi, R. Kramer, P. Berard, and R. J. Wood, "Hyperelastic pressure sensing with a liquid-embedded elastomer," *J. Micromech. Microeng.*, vol. 20, no. 12, 2010.

[15] Y.-L. Park, B. Chen, and R. J. Wood, "Design and fabrication of soft artificial skin with using embedded microchannels and liquid conductors," *IEEE Sens. J.*, vol. 12, no. 8, pp. 2711–2718, 2012.

[16] V. Giurgiutiu and A. N. Zagrai, "Embedded self-sensing piezoelectric wafer active sensors for structural health monitoring," *Trans. ASME, J. Vibr. Acoust.*, vol. 124, no. 1, pp. 116–125, 2002.

[17] A. Kadowaki, "Development of soft sensor exterior embedded with multi-axis deformable tactile sensor system," in *Proc. IEEE Int. Symp. Rob. Hum. Interact. Commun.*, Toyama, Japan, September 2009, pp. 1093–1098.

[18] Y.-L. Park, S. C. Ryu, R. J. Black, K. Chau, B. Moslehi, and M. R. Cutkosky, "Exoskeletal force-sensing end-effectors with embedded optical fiber-bragg-grating sensors," *IEEE Trans. Rob.*, vol. 25, no. 6, pp. 1319–1331, December 2009.

[19] Y.-L. Park, S. Elayaperumal, B. Daniel, S. C. Ryu, M. Shin, J. Savall, R. J. Black, B. Moslehi, and M. R. Cutkosky, "Real-time estimation of 3-d needle shape and deflection for mri-guided interventions," *IEEE/ASME Trans. Mechatron.*, vol. 15, no. 6, pp. 906–915, December 2010.

[20] C.-P. Chou and B. Hannaford, "Measurement and modeling of mckibben pneumatic artificial muscles," *IEEE Trans. Rob. Autom.*, vol. 12, no. 1, pp. 90–102, Feb. 1996.

[21] R. J. Whitney, "The measurement of changes in human limb-volume by means of a mercury-in-rubber strain gage," *Proc. Physiol. Soc*, vol. 109, pp. 5–6, 1049.

[22] M. Wehner, Y.-L. Park, C. Walsh, R. Nagpal, R. J. Wood, T. Moore, and E. Goldfield, "Experimental characterization of components for active soft orthotics," in *Submitted in Proc. IEEE Int. Conf. Biomed. Rob. Biomechatron.*, Roma, Italy, June 2012.